# Morphological tuning, self-assembly and optical properties of indium oxide nanocrystals†

**Enyi Ye,[a] Shuang-Yuan Zhang,[ab] Suo Hon Lim,[a] Shuhua Liu[ab] and Ming-Yong Han*[ab]**

*Received 6th April 2010, Accepted 11th August 2010*
**DOI: 10.1039/c0cp00138d**

In this paper, weak acids, weak bases or their mixtures were used as reaction media/coordinating ligands to achieve systematic morphological control over amphoteric indium oxide nanostructures. Different indium/oleic acid molar ratios from 1 : 0, 1 : 1, 1 : 2, 1 : 3, 1 : 6 and 1 : 15 in non-coordinating, weakly coordinating, strongly coordinating and their mixed media were adopted to prepare irregular aggregated nanoparticles and uniform regular/truncated octahedra, *etc*. In addition to their strong size-dependent absorption, single-crystalline indium oxide octahedra also gave a strong band-edge emission while irregular indium oxide aggregated nanoparticles only exhibited a weak deep-trap emission. Meanwhile, the truncated octahedra were self-assembled into either zigzag lines or pentagram patterns, and the regular octahedra and truncated cubes were self-assembled into hexagonally packed nanocrystal arrays. In addition, the formation mechanism of the various nanostructures under different conditions was investigated in detail.

## Introduction

Various indium oxide nanostructures including nanoparticles,[1,2] nanowires[3–5] and nanotubes[6] have recently been synthesized in vapor, liquid and solid phases. Due to the bixbyite-type cubic structure of indium oxide, it is also expected to produce euhedral isometric nanocrystals including various cubes, octahedra or dodecahedra by developing new synthetic strategies and optimizing reaction conditions.[7–9] Similar to zinc oxide, indium oxide is amphoteric, and its formation can thus be greatly influenced by the acidic or basic properties of reaction media/coordinating ligands.[10,11] Based on these properties, weak organic acids, weak organic bases or their mixtures can be selectively used to achieve systematic morphological control over amphoteric indium oxide nanostructures. In this paper, various morphology-tuned indium oxide nanocrystals were obtained by using fatty acids (*e.g.* oleic acid), fatty amines (*e.g.* trioctylamine) or their mixtures. Different molar ratios of indium:oleic acid from 1 : 0, 1 : 1, 1 : 2, 1 : 3, 1 : 6 and 1 : 15 were adopted systematically to prepare various indium oxide nanoshapes including irregular aggregated nanoparticles and uniform regular/truncated octahedra in non-coordinating, weakly coordinating, strongly coordinating and their mixed media. In addition to their strong size-dependent absorption, single-crystalline indium oxide octahedra also give a strong band-edge emission while irregular indium oxide aggregated nanoparticles only exhibit a weak deep-trap emission. In addition to short-wavelength optical applications of semiconducting indium oxide nanocrystals, these uniform faceted nanocrystals could also be used as building blocks to achieve various non-close stacking nanocrystal self-assemblies, which would be useful to fabricate devices for gas/biosensing, optical/antistatic coatings, infrared reflectors, transistors, displays, photovoltaic, batteries, *etc.*[12–17]

## Experimental

### Chemicals

Indium(III) acetate ($InAc_3$, 99%), oleic acid (OA, 70%), oleylamine (OAm, 70%), trioctylamine (TOA, 98%), and 1-octyldecene (ODE, 90%) were purchased from Sigma-Aldrich and used without further purification. All synthetic experiments were conducted using a Schlenk line under an inert argon atmosphere.

### Thermolytic preparation of indium oxide nanoparticles in OA

Under magnetic stirring and heating to 90 °C, 1.0 mmol $InAc_3$ was dissolved in 5.0 mL OA to form 1.0 mmol indium oleate. The resulting colorless solution was then degassed under vacuum at 90 °C for 15 min followed by quickly heating to 340 °C. By maintaining at this temperature for 60 min, a milky white solution was obtained. After cooling to room temperature, 15 mL hexane was mixed into the reaction system followed by the addition of 30 mL ethanol to precipitate out the crude product. After recovery by centrifugation, the white product was dispersed in 15 mL hexane followed by another two rounds of purification. The as-purified product was easily dispersed in 15 mL hexane for further use.

---

[a] *Institute of Materials Research and Engineering, Agency for Science, Technology and Research, 3 Research Link, Singapore 117602. E-mail: my-han@imre.a-star.edu.sg; Fax: (65) 6872 0785; Tel: (65) 6874 1987*
[b] *Division of Bioengineering, National University of Singapore, 9 Engineering Drive 1, Singapore 117576*

† Electronic supplementary information (ESI) available: Figs. S1–S3. See DOI: 10.1039/c0cp00138d

### Thermolytic preparation of indium oxide nanoparticles in ODE, TOA, or their mixture

Under magnetic stirring and heating to 90 °C, 1.0 mmol $InAc_3$ was dissolved in mixed 1.0 mL OA and 4.0 mL ODE (or TOA) to form 1.0 mmol indium oleate. The resulting colorless solution was then degassed under vacuum at 90 °C for 15 min followed by quickly heating to 320 °C. By maintaining at this temperature for 30 min, a milky white solution was obtained. The purification steps were the same as those described above.

The preparation of indium oxide nanoparticles in ODE (or TOA) with different In:OA molar ratios from 1 : 1, 1 : 2, 1 : 3 to 1 : 6 (Table 1) were also carried out at 320 °C while other experimental conditions remained unchanged. Meanwhile, the optimized preparation of uniform indium oxide nanoparticles was also conducted at 320 °C in mixed 2.0 mL ODE and 2.0 mL TOA. The purification steps were the same as those described above. It is noted that the total volume of solvent added was maintained at 5.0 mL for these preparations.

### Aminolytic preparation of indium oxide nanoparticles in ODE

Under magnetic stirring and heating to 90 °C, 1.0 mmol $InAc_3$ was dissolved in mixed 1.0 mL OA and 4.0 mL ODE to form 1.0 mmol indium oleate. The resulting colorless solution was then degassed under vacuum at 90 °C for 15 min followed by quickly heating to 320 °C. After the quick injection of 1.0 or 3.0 mmol oleylamine (OAm), a milky white solution was obtained within 15 min. The purification steps were the same as those described above.

### Characterization

TEM and high-resolution TEM (HRTEM) images were examined using JEOL 1010 (100 kV) and JEM 2100 (200 kV) transmission electron microscopes, respectively. TEM samples were prepared by placing a drop of indium oxide nanoparticle dispersion in hexane onto carbon-coated copper grids followed by drying. X-Ray diffraction (XRD) patterns were measured by using a Bruker D8 general area detector diffraction system (GADDS) under Cu Kα radiation. XRD samples were prepared by dropping indium oxide nanoparticle dispersion in hexane onto a silicon (100) wafer and further drying in air so as to have the same nanocrystal orientations as that in the TEM samples. Fluorescence and absorption spectra were recorded on a SHIMADZU RF-5301PC spectrofluorophotometer and a SHIMADZU UV-1601 UV–visible spectrophotometer, respectively.

## Results and discussion

### Thermolytic reaction of indium oleate in OA, ODE or TOA

First, 1.0 mmol $InAc_3$ reacted with ~3.0 mmol of 1.0 mL OA under heating to 90 °C. The resulting 1.0 mmol indium oleate was thermally decomposed at 340 °C for 1 h in the remaining 4.0 mL OA (~12.0 mmol) to form indium oxide nanoparticles of ~60 nm in size, which contained a majority of truncated octahedral nanoparticles (Fig. 1A). The corresponding XRD pattern in Fig. 1D shows the main diffraction peaks at 21.48°, 30.58°, 35.44°, 50.94° and 60.60°, which are assigned to the (211), (222), (400), (440) and (622) reflections of body-centred cubic indium oxide (JCPDS 76-0152), respectively. Moreover, no peak from impurities was observed in the obtained nanoparticles.

Instead of 4.0 mL OA, the thermolytic reaction of 1.0 mmol indium oleate was conducted in 4.0 mL ODE at 320 °C for 30 min. Regular octahedral indium oxide nanoparticles of ~60 nm in size (Fig. 1B and E) were obtained instead under the reduced protection using only 3.0 mmol oleate in the absence of excessive OA. Instead of 4.0 mL OA, the thermolytic reaction of 1.0 mmol indium oleate was also conducted in 4.0 mL TOA at 320 °C for 30 min. Truncated cubic indium oxide nanoparticles of ~40 nm in size (Fig. 1C and F) were obtained due to the competitive surface-coordination of a larger amount of weakly coordinating 4.0 mL TOA to 3.0 mmol oleate. In overall, the reaction medium-dependent morphology-tuned preparation of various indium oxide nanostructures in Fig. 1A–C was demonstrated by the thermolytic reaction of indium oleate in non-coordinating ODE, weakly coordinating TOA and strongly coordinating OA.

### In:OA molar ratio-dependent morphological tuning in ODE

In pure 5 mL OA (In:OA = 1 : 15), non-uniform indium oxide octahedra were formed, and most of them were clearly truncated. In this case, 1.0 mmol $InAc_3$ was completely converted to $In(oleate)_3$ by reacting with 3.0 mmol OA, and the large excess of 12.0 mmol OA was left to strengthen the surface protection of indium oxide nanoparticles on the ⟨001⟩

**Table 1** Morphology-controlled synthesis of various indium oxide nanostructures

| Samples | In:OA (molar ratio) | $InAc_3$/mmol | OA/mL | ODE/mL | TOA/mL | OAm/mmol | Morphology |
|---|---|---|---|---|---|---|---|
| 1 | 1 : 15 | 1.0 | 5.0 | — | — | — | Truncated octahedral nanoparticles |
| 2 | 1 : 6 | 1.0 | 2.0 | 3.0 | — | — | Regular octahedral nanoparticles |
| 3 | 1 : 3 | 1.0 | 1.0 | 4.0 | — | — | Regular octahedral nanoparticles |
| 4 | 1 : 2 | 1.0 | 0.67 | 4.33 | — | — | Irregular nanoparticles |
| 5 | 1 : 1 | 1.0 | 0.33 | 4.67 | — | — | Irregular nanoparticles |
| 6 | 1 : 6 | 1.0 | 2.0 | — | 3.0 | — | Multi-faceted nanoparticles |
| 7 | 1 : 3 | 1.0 | 1.0 | — | 4.0 | — | Truncated cubic nanoparticles |
| 8 | 1 : 2 | 1.0 | 0.67 | — | 4.33 | — | Irregular nanoparticles |
| 9 | 1 : 1 | 1.0 | 0.33 | — | 4.67 | — | Irregular nanoparticles |
| 10 | 1 : 0 | 1.0 | — | — | 5.0 | — | Irregular nanoparticles |
| 11 | 1 : 3 | 1.0 | 1.0 | 2.0 | 2.0 | — | Regular octahedral nanoparticles |
| 12 | 1 : 3 | 1.0 | 1.0 | 4.0 | — | 1.0 | Multi-faceted nanoparticles |
| 13 | 1 : 3 | 1.0 | 1.0 | 4.0 | — | 3.0 | Irregular nanoparticles |

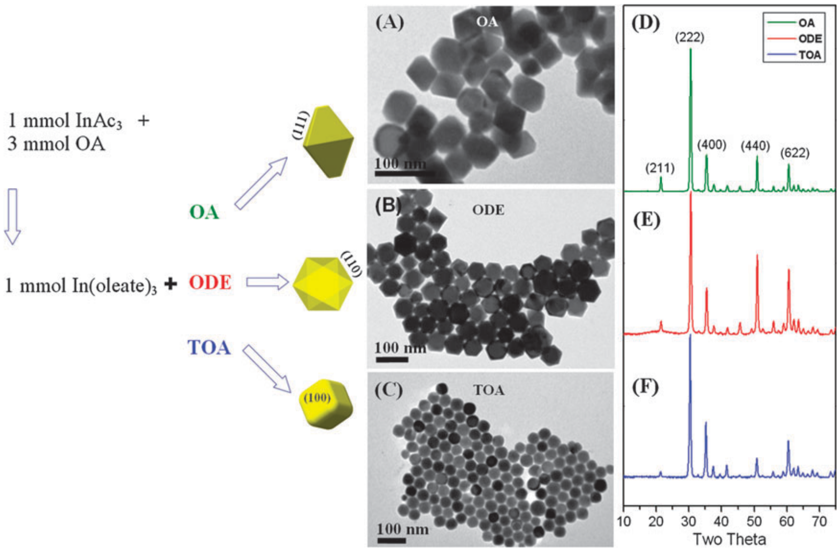

**Fig. 1** TEM images of the reaction medium-dependent morphology-tuned indium oxide nanoparticles prepared by the thermolytic reaction of 1.0 mmol indium oleate in (A) 4.0 mL OA, (B) 4.0 mL ODE, and (C) 4.0 mL TOA. Schematic illustration of the morphological change in OA, ODE, and TOA is shown on the top left of this figure. (D)–(F) The corresponding X-ray diffraction patterns of various indium oxide nanostructures that are schematically illustrated for the reaction medium-dependent morphological evolution in the left of this figure.

direction for the formation of truncated octahedral nanostructures. As a result, they preferred to lie down to expose their rhombohedral side-view on the substrate, as shown in Fig. 1A.

When replacing 60% OA by volume with 3.0 mL ODE (In:OA = 1 : 6), non-uniform regular indium oxide octahedra were formed (Fig. 2A and Fig. S1 of the ESI†). In this case, 1.0 mmol InAc$_3$ was completely converted to In(oleate)$_3$ by reacting with 3.0 mmol OA, and a 3.0 mmol excess of OA was left. The reduction in In:OA from 1 : 15 to 1 : 6 was simply achieved by the dilution of the strongly coordinating OA with the non-coordinating ODE, and the weakened surface protection led to the formation of no truncated octahedral nanostructures.

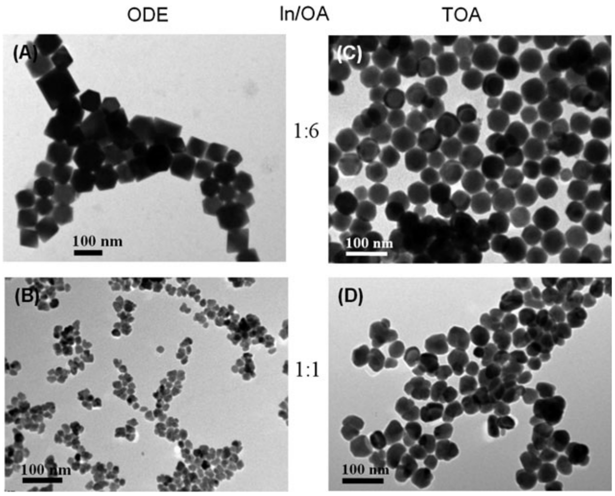

**Fig. 2** TEM images of indium oxide nanoparticles prepared by the thermolytic reaction of 1.0 mmol indium oleate in ODE with an In:OA molar ratio of (A) 1 : 6 and (B) 1 : 1, and in TOA with an In:OA molar ratio of (C) 1 : 6 and (D) 1 : 1. The total volume of solvent added was maintained at 5.0 mL for the preparations (Table 1).

When replacing 80% OA by volume with 4.0 mL ODE (In:OA = 1 : 3), uniform regular indium oxide octahedra were produced (Fig. 1B). In this case, 1.0 mmol InAc$_3$ was completely converted to In(oleate)$_3$ by reacting with 3.0 mmol OA, and no excess of OA was left. Irregular indium oxide nanoparticles were obtained (Fig. 2B and Fig. S1 of the ESI†) when a lower amount of OA (In:OA = 1 : 1 or 1 : 2) was used to form partially coordinated indium oleate (InAc$_3$ → InAc$_2$(oleate)$_1$ or InAc$_1$(oleate)$_2$) with 2.0 or 1.0 mmol of unreacted Ac remaining. The non-faceted growth of indium oxide nanoparticles was caused by the insufficient surface protection when In:OA is 1 : 1 or 1 : 2. In comparison, In:OA = 1 : 3 is the optimum condition to achieve a good morphological control of regular indium oxide octahedra due to appropriate surface protection of indium oxide nanoparticles.

### In:OA molar ratio-dependent morphological tuning in TOA

When a smaller amount of OA (In:OA = 1 : 1 or 1 : 2) was used in weakly coordinating >4.0 mL TOA, irregular indium oxide nanoparticles were obtained (Fig. 2C and Fig. S2 of the ESI†) with 2.0 or 1.0 mmol unreacted Ac remaining. The non-faceted growth of indium oxide nanoparticles was caused by the insufficient surface protection at In:OA = 1 : 1 or 1 : 2. When In:OA = 1 : 3 was used to form 1.0 mmol indium oleate without the excess OA, the competitive coordination of a large amount of 4.0 mL TOA to 3.0 mmol oleate led to the formation of truncated cubic indium oxide nanoparticles (Fig. 1C). Moreover, when more strongly coordinating OA (In:OA = 1 : 6) was used to provide stronger surface protection, multi-faceted indium oxide nanoparticles were formed (Fig. 2D and Fig. S2 of the ESI†).

## Roles of tertiary and primary alkyl amines in forming indium oxide nanostructures

Experimentally, 1.0 mmol InAc$_3$ was also dissolved into weakly coordinating 5.0 mL TOA (In:OA = 1 : 0), and the thermolytic reaction of resulting weak TOA-coordinated indium complexes as compared to indium oleate was much quicker to form smaller indium oxide nanoparticles, which were further aggregated into larger irregular nanoparticles (composed of smaller nanoparticles of $<$10 nm in average size as shown in Fig. S3†) due to the weak surface protection of TOA.

In 5.0 mL tertiary alkyl amine (R–N–R$_2$), TOA, the thermolytic reaction of 1.0 mmol indium acetate or indium oleate can form indium oxide nanostructures at a temperature of $>$300 °C. In 5.0 mL primary alkyl amine (R–N–H$_2$), oleylamine, –NH$_2$ groups can nucleophilically attack the –C=O in acetate or oleate (S$_N$2 reaction) to form an organic amide, accelerating the formation of indium oxide at a temperature of less than 300 °C (*e.g.* 260 °C). The aminolytic reaction for preparing nano-sized metal oxides including zinc oxide and titanium dioxide was reported in our previous research and by other groups.[18–22]

In order to further understand the function of the primary amine, 3.0 mmol primary oleylamine was added to aminolyze 1.0 mmol indium oleate, In(oleate)$_3$ in non-coordinating 4.0 mL ODE. After the complete consumption of 3.0 mmol oleate by reacting with 3.0 mmol oleylamine, only irregular indium oxide nanoparticles aggregates (Fig. 3A) were quickly produced due to the absence of the surface protection by oleate. Accordingly, the use of 1.0 mmol oleylamine only consumed 1.0 mmol oleate in 1.0 mmol indium oleate, and the remaining 2.0 mmol oleate played a role in the surface protection for the formation of multi-faceted indium oxide nanoparticles (Fig. 3B).

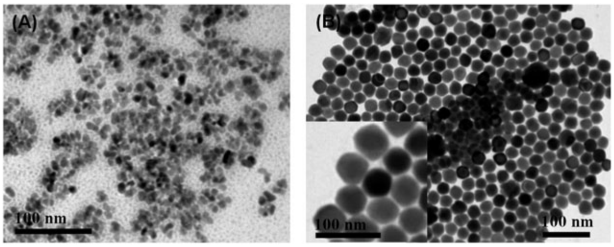

**Fig. 3** TEM images of indium oxide nanoparticles prepared by the aminolytic reaction of 1.0 mmol indium oleate in 4.0 mL ODE at a molar ratio of In:OA = 1 : 3 after the addition of (A) 3.0 mmol oleylamine and (B) 1.0 mmol oleylamine.

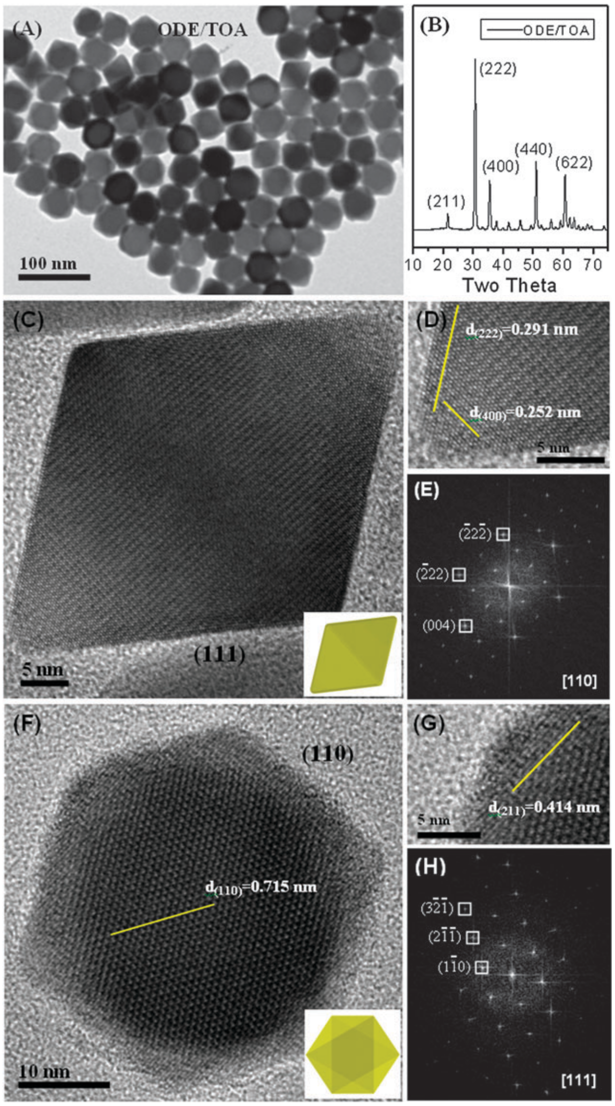

**Fig. 4** (A) TEM image and (B) XRD pattern of indium oxide octahedra with two orientations prepared by the thermolytic reaction of 1.0 mmol indium oleate in mixed 2.0 mL ODE and 2.0 mL TOA. (C, D) HRTEM images and (E) FFT pattern of a single-crystalline indium oxide octahedron (rhombohedral shape) viewed along the [110] zone axis. (F, G) HRTEM images and (H) FFT pattern of a single-crystalline indium oxide octahedron (hexagonal shape) viewed along the [111] zone axis.

## Optimized fabrication of indium oxide nanocrystals in mixed ODE and TOA

By complementary adoption of the dilution effect of non-coordinating ODE and the coordination effect of weakly coordinating TOA, very uniform regular octahedral indium oxide nanostructures of ~50 nm in size (Fig. 4A and B) were produced in mixed 4.0 mL ODE–TOA (1 : 1 in volume) when using the optimized molar ratio of In:OA = 1 : 3. The TEM images showed two different orientations of indium oxide octahedra on a carbon film along the [110] and the [111] zone axes as given in Fig. 4C and F, respectively.

An HRTEM image of a rhombohedral-shaped indium oxide nanocrystal viewed along the [110] zone axis is shown in Fig. 4C. The crystal lattice is across the whole nanocrystal and the lattice spacing of 0.291 nm in Fig. 4D corresponds to the *d*-spacing of the (222) planes of cubic indium oxide. Fig. 4E shows its corresponding fast Fourier transform (FFT) pattern, where a few bright spots are indexed to the $(\bar{2}2\bar{2})$, $(\bar{2}22)$ and (004) planes.

The HRTEM image of a hexagonal-shaped indium oxide nanocrystal viewed along the [111] zone axis is revealed in Fig. 4F. The lattice spacing of 0.715 nm corresponds to the *d*-spacing of the (110) planes of cubic indium oxide (Fig. 4F).

The lattice spacing of 0.414 nm at the thinner edge corresponds to the *d*-spacing of the (211) planes of cubic indium oxide (Fig. 4G). Their corresponding FFT spots in Fig. 4H are indexed to the $(3\bar{2}\bar{1})$, $(2\bar{1}\bar{1})$ and $(1\bar{1}0)$ planes.

## Optical properties

The uniform indium oxide octahedral nanocrystals of ~50 nm in size prepared in mixed ODE–TOA exhibited a strong UV absorption at ~300 nm (Fig. 5A) the corresponding band-edge UV emission (Fig. 5B) at ~367 nm was also very strong, accompanying a weak emission in the visible spectral region. Like what was observed in zinc oxide nanostructures,[18] the weak photoluminescence of indium oxide nanostructures in the visible spectral region was ascribed to some defects in the crystal lattice of indium oxide nanocrystals, mainly from oxygen vacancies.

Iirregular indium oxide nanostructures prepared by the thermolytic reaction of 1.0 mmol $InAc_3$ in 5.0 mL TOA also exhibited a strong UV absorption at ~258 nm (Fig. 5C); however, the corresponding band-edge UV emission is very weak (Fig. 5D), accompanying a stronger deep-trap emission in the visible spectral region.[23] As shown in Fig. S3,† the irregular indium oxide nanostructures of <30 nm in size were also composed of smaller nanoparticles of <10 nm in average size, indicating their aggregation-driven formation may generate more defects to show the stronger deep-trap emission. Due to size effects, smaller indium oxide nanoparticles of <10 nm in size from the irregular nanostructures of <30 nm in size have a strong absorption centred at ~258 nm; larger indium oxide octahedral nanoparticles of ~50 nm in size have a red-shifted strong absorption centred at ~300 nm, accompanying a long tail in the visible spectral region.

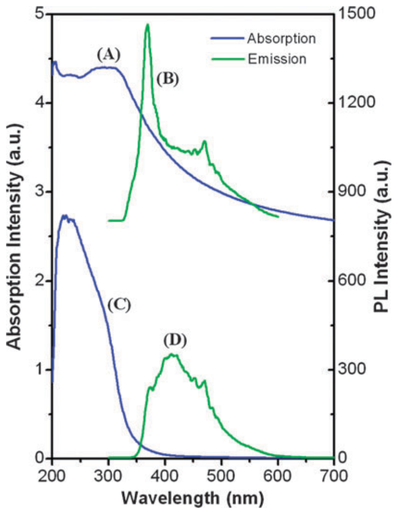

**Fig. 5** (A) UV–visible absorption and (B) photoluminescence spectra of as-purified octahedral indium oxide nanoparticles in hexane after preparing in mixed 2.0 mL ODE and 2.0 mL TOA. (C) UV–visible absorption and (D) photoluminescence spectra of as-purified irregular indium oxide nanoparticles in hexane after preparing in 5.0 mL TOA. The photoluminescence spectra were recorded under an excitation at 258 nm.

## Self-assemblies of octahedral indium oxide prepared in OA

As shown in Fig. 1A, most of the resulting indium oxide octahedra prepared by the thermolytic reaction of 1.0 mmol indium oleate in 4.0 mL OA were clearly truncated, and they preferred to lie down to exhibit their rhombohedral side view. When slowly evaporating their concentrated hexane solution on copper grids, the truncated octahedra stacked randomly. When slowly evaporating their diluted hexane solution on copper grids, the truncated octahedra self-assembled themselves into either a zigzag line or a pentagram shape, as shown in Fig. 6. Zigzag assemblies were not occasional cases and three examples are given in Fig. 6B–D. Interestingly, randomly packed octahedra were also observed at the two ends of the zigzag assemblies. Pentagram assemblies were also observed in Fig. 6F–H. The projected rhombohedral shape viewed along the [110] zone axis of octahedra exhibited each small angle is ~72° in the pentagram assembly comprising of five octahedra ($5 \times 72° = 360°$). The close face-to-face contact between their (111) planes between adjacent octahedra through hydrophobic–hydrophobic interaction of surface-coordinated oleate can form different self-assembled patterns.

## Self-assemblies of octahedral and cubic indium oxide prepared in mixed TOA and ODE

As shown in Fig. 7A and B, regular indium oxide octahedra prepared by the thermolytic reaction of 1.0 mmol indium oleate in 4.0 mL mixed ODE–TOA (1 : 1 in volume) were self-assembled into a hexagonally packed nanocrystal array instead. Regular octahedra that are composed of eight equilateral triangles allow one of the eight equivalent faces to sit on the substrate, and almost all the regular octahedra give their hexagonal view (a minority shows their rhombohedral

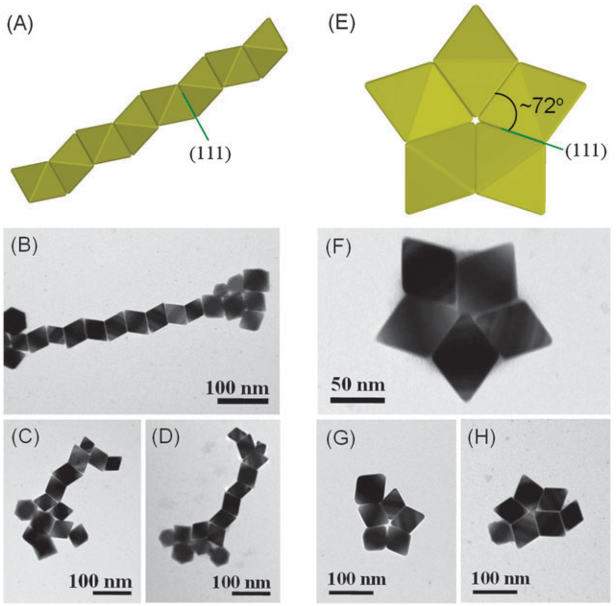

**Fig. 6** Schematic and TEM images of zigzag (A–D) and pentagram (E–H) self-assemblies of oleate-capped truncated indium oxide octahedral nanocrystals as prepared by the thermolytic reaction of 1.0 mmol indium oleate in 4.0 mL OA.

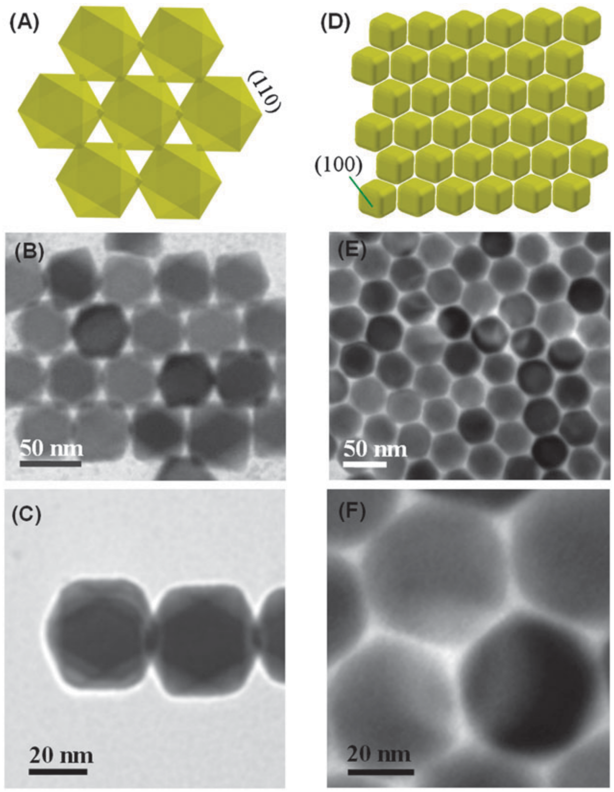

**Fig. 7** Schematic and TEM images of hexagonally packed self-assemblies of TOA-capped indium oxide octahedra (A, B, C) and cubes (D, E, F) as prepared by the thermolytic reaction of 1.0 mmol indium oleate in 4.0 mL ODE–TOA and 4.0 mL TOA, respectively.

view) as shown in Fig. 4A, 7B and C. The resulting projected hexagonal shape viewed along the [111] zone axis of the octahedra is shown in Fig. 7C. The adjacent octahedra interact with each other through the (111) planes of their thinner corners. As shown in Fig. 7D–F, heavily truncated indium oxide cubes prepared by the thermolytic reaction of 1.0 mmol indium oleate in 4.0 mL TOA tended to sit their heavily truncated (111) corners on the substrate along the ⟨111⟩ direction, and they further contact each other through the truncated (111) corners (vertices) to form a hexagonally packed nanocrystal array (Fig. 7D and E).

### Self-assemblies of surface-capped multi-faceted nanocrystals

Monodisperse spherical nanoparticles prefer to assemble themselves into hexagonal close-packing (hcp) or cubic close-packing (ccp), which are usually realized through hydrophobic–hydrophobic interaction between the surface-coated long alkyl chain ligands from adjacent nanoparticles. Similarly, short nanorods with uniform round cross-sections are often self-assembled into hexagonal close stacking as well.

In comparison, non-spherical nanoparticles used as building blocks to achieve self-assembly depend on their monodispersity not only in size but also in shape. No matter what size the uniform non-spherical nanoparticles have, neutral metal nanoparticles like silver nanocubes[24–26] and low-valence metal oxide nanoparticles like $Cu_2O$ dodecahedra of $> 200$ nm took close cubic or hexagonal packing.[27] For high-valence metal oxide nanoparticles, smaller non-spherical ones of less than 20 nm like $Fe_3O_4$ nanocubes or $In_2O_3$ octahedra often took close stacking to form superlattice structures.[8,28] In our case, much larger faceted $In_2O_3$ octahedra of more than 50 nm in size were synthesized and non-close stacking was achieved instead through edge–edge stacking rather than face–face interactions between adjacent larger non-spherical nanostructures. Their large crystallographic planes of high-valence metal oxide nanoparticles are either neutral or strongly positive/negative charged. The latter one can cause strong electrostatic repulsion between the highly charged large crystallographic planes from adjacent nanoparticles, resulting in non-close-packed arrays.

For example, oleate-capped $In_2O_3$ octahedra as prepared by the thermal decomposition of 1.0 mmol indium oleate in 4.0 mL OA was self-assembled into either a zigzag line or a pentagram shape through close contact between neutral (111) planes from adjacent truncated octahedra, as shown in Fig. 6. In comparison, TOA-coated $In_2O_3$ octahedra as prepared by the thermal decomposition of 1.0 mmol indium oleate in mixed 2.0 mL ODE–2.0 mL TOA (the reaction of 1.0 mmol $InAc_3$ with ∼3.0 mmol OA can form 1.0 mmol indium oleate, and the remaining ∼3.0 mmol $H^+$ can be bound to TOA to form positively charged TOA, $R_3NH^+$.) were self-assembled into hexagonally packed nanocrystal arrays of regular octahedral nanocrystals (Fig. 7). However, only hexagonal loose-packing was achieved, and this is different from the hexagonal close-packing (hcp) of spherical nanoparticles or small non-spherical nanoparticles. Also, TOA-capped octahedral nanocrystals were self-assembled without direct contact of (111) planes; in contrast, oleate-capped octahedral nanocrystals were self-assembled by direct contact of (111) planes. The difference in self-assembling oleate-capped and TOA-capped octahedral nanocrystals is attributed to their difference in surface charging to form different assembled patterns.

As shown in Fig. 8A, each octahedral nanocrystal exposes eight equivalent (111) surfaces externally, which are filled with $O^{2-}$ and $In^{3+}$ with an atomic ratio of 3 : 2 to form neutral surfaces. After capping with oleate, the octahedral nanocrystals have neutral (111) faces to assemble themselves by hydrophobic–hydrophobic interaction of oleate on the surface. After capping with TOA, the octahedral nanocrystals have positive-charged (111) faces to generate electrostatic repulsion between adjacent nanoparticles. In a similar way, TOA-$H^+$ capped on the neutral (110) edges (Fig. 8B) also generate electrostatic repulsion between the edges of adjacent octahedral nanoparticles, thus vertice–vertice (111) contact of two adjacent octahedra has the smallest overlapping to minimize the electrostatic repulsion and further reduce the self-assembled system energy.

Following this reasoning, hexagonally packed nanocrystal arrays of large cubic nanocrystals of ∼40 nm were also achieved without direct contact between (100) faces. This is due to the strong electrostatic repulsion between the highly negatively charged (100) faces of adjacent indium oxide nanocubes as shown in Fig. 8C. The weak positive charge from surface-bound TOA slightly affects the surface charging and further self-assembly behavior. The direct

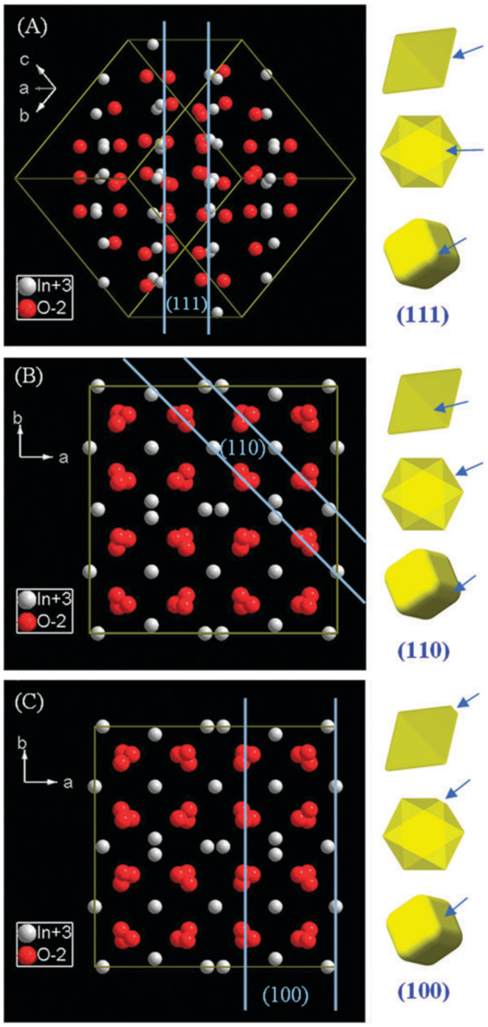

**Fig. 8** Schematic atomic arrangement of $O^{2-}$ and $In^{3+}$ on the (111), (110) and (100) planes of indium oxide nanostructures.

edge–edge/corner–corner contact of neutral (110) and (111) faces has the minimum electrostatic repulsion to form non-close contacts as shown in Fig. 7.

## Conclusions

In summary, morphology-tuned indium oxide nanostructures were systematically prepared by alternatively using weak organic acids, weak organic bases or their mixture as coordinating ligands/reaction media. Different In:OA molar ratios from 1 : 0, 1 : 1, 1 : 2, 1 : 3, 1 : 6 and 1 : 15 were also used to prepare irregularly aggregated nanoparticles and uniform cubes and octahedra in non-coordinating ODE, weakly coordinating TOA, strongly coordinating OA and their mixed media. The single-crystalline indium oxide octahedra gave an intense UV band-edge emission; in contrast, irregular indium oxide nano-aggregates only exhibited a weak deep-trap visible emission. In addition to short-wavelength optical applications, these uniform polyhedral nanocrystals were also be used as building blocks for achieving various non-close self-assembled patterns.

## Acknowledgements

This work was financially supported by the Institute of Materials Research & Engineering and the National University of Singapore.

## References

1 W. K. Seo, H. H. Jo, K. Lee and J. T. Park, *Adv. Mater.*, 2003, **15**, 795.
2 Q. S. Liu, W. G. Lu, A. H. Ma, J. K. Tang, J. Lin and J. Y. Fang, *J. Am. Chem. Soc.*, 2005, **127**, 5276.
3 W. Wan, M. Wei, D. Zhi, J. L. MacManus-Discoll and M. G. Blamire, *Adv. Mater.*, 2006, **18**, 234.
4 C. H. Liang, G. W. Meng, Y. Lei, F. Phillipp and L. D. Zhang, *Adv. Mater.*, 2001, **13**, 1330.
5 M. J. Zheng, L. D. Zhang, G. H. Li, X. Y. Zhang and X. F. Wang, *Appl. Phys. Lett.*, 2001, **79**, 839.
6 C. L. Chen, D. R. Chen, X. L. Jiao and C. Q. Wang, *Chem. Commun.*, 2006, 4632.
7 O. Medenbach and H. Wilk, *The Magic of Minerals*, Springer, New York, 1986.
8 B. G. Hyde and S. Andersson, *Inorganic Crystal Structures*, Wiley, New York, 1989.
9 W. Lu, Q. Liu, Z. Sun, J. He, C. Ezeolu and J. Fang, *J. Am. Chem. Soc.*, 2008, **130**, 6983.
10 D. F. Shriver and P. W. Atkins, *Inorganics Chemistry*, Oxford University Press, New York, 1999.
11 M. Niederberger, *Acc. Chem. Res.*, 2007, **40**, 793.
12 A. Prim, E. Pellicer, E. Rossinyol, F. Peiró, A. Cornet and J. R. Morante, *Adv. Funct. Mater.*, 2007, **17**, 2957.
13 M. Curreli, C. Li, Y. H. Sun, B. Lei, M. A. Gundersen, M. E. Thompson and C. W. Zhou, *J. Am. Chem. Soc.*, 2005, **127**, 6922.
14 P. Nguyen, H. T. Ng, T. Yamada, M. K. Smith, J. Li, J. Han and M. Meyyappan, *Nano Lett.*, 2004, **4**, 651.
15 D. W. Kim, I. S. Hwang, S. J. Kwon, H. Y. Kang, K. S. Park, Y. J. Choi, K. J. Choi and J. G. Park, *Nano Lett.*, 2007, **7**, 3041.
16 N. Naghavi, C. Marcel, L. Dupont, A. Rougier, J. B. Leriche and C. J. Guery, *J. Mater. Chem.*, 2000, **10**, 2315.
17 I. Hamberg and C. G. Granqvist, *J. Appl. Phys.*, 1986, **60**, R123.
18 Z. H. Zhang, S. H. Liu, S. Y. Chow and M. Y. Han, *Langmuir*, 2006, **22**, 6335.
19 Z. H. Zhang, X. H. Zhong, S. H. Liu, D. F. Li and M. Y. Han, *Angew. Chem., Int. Ed.*, 2005, **44**, 3466.
20 H. M. Wu, Y. G. Yang and Y. C. Cao, *J. Am. Chem. Soc.*, 2006, **128**, 16522.
21 Y. W. Jun, J. S. Choi and J. Cheon, *Angew. Chem., Int. Ed.*, 2006, **45**, 3414.
22 X. Chen and S. S. Mao, *Chem. Rev.*, 2007, **107**, 2891.
23 H. Q. Cao, X. Q. Qiu, Y. Liang and Q. M. Zhu, *Appl. Phys. Lett.*, 2003, **83**, 761.
24 A. Demortière, P. Launois, N. Goubet, P. A. Albouy and C. Petit, *J. Phys. Chem. B*, 2008, **112**, 14583.
25 A. R. Tao, S. Habas and P. D. Yang, *Small*, 2008, **4**, 310.
26 Y. Xia, Y. Xiong, B. Lim and S. E. Skrabalak, *Angew. Chem., Int. Ed.*, 2009, **48**, 60.
27 K. X. Yao, X. M. Yin, T. H. Wang and H. C. Zeng, *J. Am. Chem. Soc.*, 2010, **132**, 6131.
28 Q. Song, Y. Ding, Z. L. Wang and Z. J. Zhang, *J. Phys. Chem. B*, 2006, **110**, 25547.